Journal of Information Hiding and Multimedia Signal Processing ©2015 ISSN 2073-4212
Ubiquitous International Volume **6**, Number **4**, July **2015**

Design and Application of Triple-Band Planar Dipole Antennas

Yuh-Yih Lu, Jun-Yi Kuo
Department of Electrical Engineering
Minghsin University of Science and Technology
Hsinchu 304, Taiwan, R.O.C.
yylu@must.edu.tw

Hsiang-Cheh Huang[1]
Department of Electrical Engineering
National University of Kaohsiung
Kaohsiung 811, Taiwan, R.O.C.
huang.hc@gmail.com

Received September 2014; revised April 2015

Abstract. *In this paper, we propose the low-profile planar triple symmetric arms dipole antennas for wireless communication applications. Three symmetric arms are etched on the metallic layer of a single sided printed circuit board to form the planar dipole antenna. For different applications, we present two antennas based on similar design concepts. For the first antenna, it can be operated at 2.45/3.5/5.8 GHz, and for the second one, it can be operated at 0.9/1.8/2.45 GHz, respectively. The size parameters of symmetric arms are changed to design and fabricate the antenna operating at these specific frequencies. We use IE3D software to design the two triple-band planar antennas and choose the better parameters to manufacture the proposed ones. We also discuss about the influences of dimension parameter of the proposed antennas on the resonant frequencies and impedance bandwidths of our implementations. Proposed antennas are small in sizes, and they can be applicable in GSM, RFID and WLAN frequency bands.*
Keywords: Symmetric arm; Planar dipole antenna; GSM; RFID; WLAN.

1. **Introduction.** There are important factors for the design of antenna in wireless communications, including compact size, lower cost, and ease of fabrication. Planar antennas possess the attractive features. Hence, many studies about planar antennas had been proposed and widely used in Wireless Local Area Network (WLAN) [1, 2, 3, 4], Radio Frequency Identification (RFID) [5, 6, 7], Worldwide Interoperability for Microwave Access (WiMAX) [8, 9, 10], Global System for Mobile Communication (GSM) [11, 12], and Ultra Wide Band (UWB) systems [13, 14, 15]. In modern wireless communication devices, they should be capable of operating at multiple frequency bands [16, 17, 18]. Therefore, relating researches have been published for multi-band planar antennas [19, 20, 21].

In this paper, based on similar concepts, we propose the implementations of two antennas; one is a simple uniplane dipole antenna with symmetric arms, and the other is a simple planar triple symmetric arms dipole (TSAD) antenna. The return loss, resonant frequency, impedance bandwidth, and radiation pattern are obtained from IE3D simulations. The lower, middle and upper arms of the proposed antennas control the

[1]Corresponding author.

resonant frequencies. The suitable geometric parameters of the symmetric arms are selected to fabricate the first antenna operating at 2.45/3.5/5.8 GHz with small size of 40.6mm×13mm×0.6mm, and to fabricate the second antenna operating at 0.9/1.8/2.45 GHz with size of 43mm×20mm×1.6mm for the applications in wireless communications. Proposed antennas can be built on a single sided printed circuit board. The single metal layer structure is suitable for mass production and reduces the manufacturing cost.

The rest of the paper is organized as follows. In Sec. 2 and Sec. 3, we present the design concept, simulations, and measurements of the first and the second antennas, respectively. In Sec. 4, we briefly address the comparisons between the two antennas presented in this paper. Finally, we give the conclusion of this paper in Sec. 5.

2. The 2.45/3.5/5.8 GHz Antenna.

2.1. **Antenna Design.** The first antenna has a compact size of 40.6mm×13mm×0.6mm. It is a planar dipole antenna, and its structure can be printed on a single metallic layer of FR4 dielectric substrate with the permittivity of 4.4 and thickness of 0.6mm. The configuration of this proposed antenna is depicted in Fig. 1. Three symmetric arms in Fig. 1 are etched on the metallic layer to create the operating frequency bands at 2.45/3.5/5.8 GHz. Points A and B are the feeding points of the planar dipole antenna. Three parameters including the lower arm length parameter L1, the middle arm length parameter L2, and the upper arm corner parameter S are adjusted to observe the variations with respect to the resonant frequency and impedance bandwidth. The dimension parameters of the proposed antenna shown in Fig. 1 are listed below.

- For the parameters in horizontal direction (x-direction): L3 = 14.5mm, L4 = 3mm, L5 = 2mm, and G = 1mm.
- For the parameters in vertical direction (y-direction): W = 10mm, W1 = 2mm, W2 = 2mm, W3 = 2mm, W4 = 2mm, W5 = 3mm, W6 = 7mm, and W7 = 1mm.

In addition, the 50 ohm coaxial connector was adopted for testing.

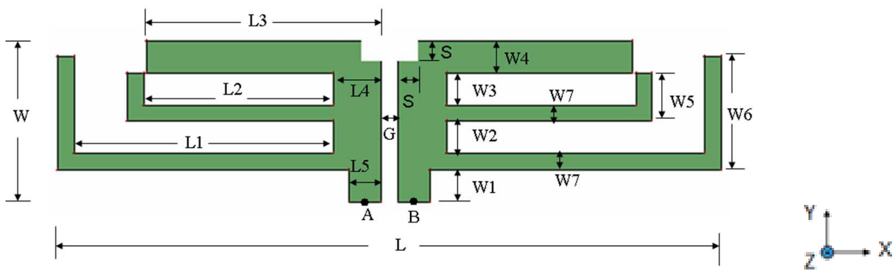

FIGURE 1. Geometry of the proposed planar dipole antenna.

2.2. **The Simulations.** We adopted various dimension parameters L1, L2 and S depicted in Fig. 1 to observe the characteristics of the first antenna. Numerical simulations and analysis for the first antenna are performed using IE3D simulation software. In order to design the proposed antenna that can be used in 2.45/3.5/5.8 GHz, we choose L1 = 16mm, L2 = 11.7mm, and S = 1mm to fabricate the triple-band planar symmetric dipole antenna. Simulation curves of return loss against frequency for varying the lower arm parameter L1 of the proposed antenna with L2 = 11.7mm and S = 1mm are depicted in Fig. 2(a). Three obvious operating frequency bands are observed in Fig. 2(a) and the lower resonant frequency is slightly decreased with increase of L1. Simulation curves of

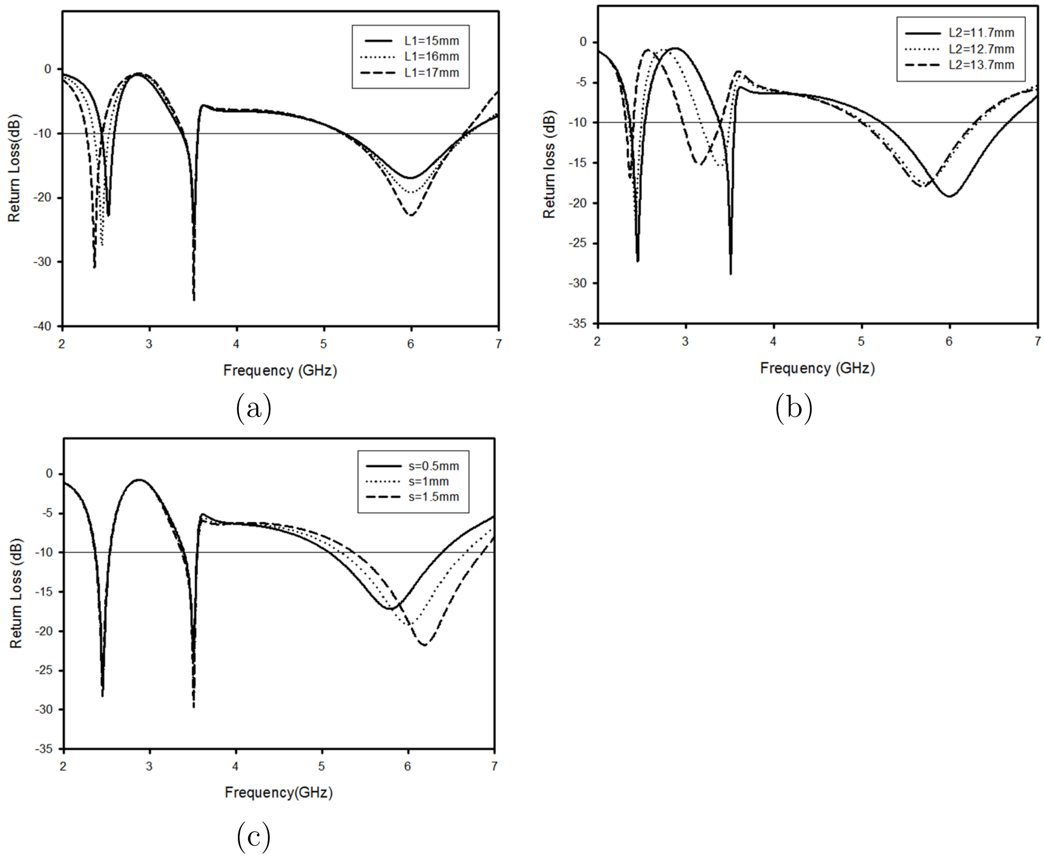

Figure 2. Simulated curves of return loss against frequency with different conditions. (a) By varying L1 with L2 = 11.7mm, and S = 1mm. (b) By varying L2 with L1 = 16mm and S = 1mm. (c) By varying S with L1 = 16mm and L2 = 11.7mm.

return loss against frequency by varying the middle arm parameter L2 with L1 = 16mm and S = 1mm, and by varying the upper arm parameter S with L1 = 16mm and L2 = 11.7mm, are depicted in Fig. 2(b) and Fig. 2(c), respectively.

From Fig. 2(b) and Fig. 2(c), three obvious operating frequency bands are also observed. The lower, middle and upper resonant frequencies are slightly decrease with the increase of L2 in Fig. 2(b). As depicted in Fig. 2(c), the lower and middle resonant frequencies are nearly unchanged while the upper resonant frequency is slightly increased with the increase of S. Simulation results, including resonant frequency (f_c), return loss (RL), and impedance bandwidth (BW), of the lower, middle, and upper operating frequency bands are listed in Table 1.

The radiation patterns are computed using IE3D software for the proposed antenna with L1 = 16mm, L2 = 11.7mm, and S = 1mm. Figs. 3(a) and 3(b) illustrate the simulated radiation patterns of $x-z$ and $y-z$ planes at 2.45 GHz, in addition, Figs. 4(a), 4(b) and Figs. 5(a), 5(b) illustrate their counterparts at 3.5 GHz and 5.8 GHz, respectively. The peak gains at the operating frequency obtained from the radiation patterns are classified as Table 2. It can be seen that the radiation patterns are almost omnidirectional in the $y-z$ plane as depicted in Figs. 3(b), 4(b), and 5(b). From the simulation results, it is easy to find that the simulated return loss, impedance bandwidth and peak gain at the lower, middle and upper frequency bands show good performance and they can be employed for 2.45/3.5/5.8 GHz applications.

Table 1. Simulated results for varying dimension parameters of the first antenna.

L1 (mm)	L2 (mm)	S (mm)	Frequency band	f_c (GHz)	RL (dB)	BW (MHz)
15.0	11.7	1.0	lower	2.53	−22.6	145
			middle	3.50	−24.2	184
			upper	6.00	−16.8	1398
16.0	11.7	1.0	lower	2.45	−27.0	170
			middle	3.50	−28.6	170
			upper	6.00	−19.1	1435
17.0	11.7	1.0	lower	2.36	−30.8	189
			middle	3.50	−35.9	161
			upper	5.96	−22.6	1389
16.0	12.7	1.0	lower	2.43	−21.7	139
			middle	3.38	−15.4	330
			upper	5.71	−17.5	1285
16.0	13.7	1.0	lower	2.37	−16.6	88
			middle	3.20	−15.1	427
			upper	5.65	−17.8	1282
16.0	11.7	0.5	lower	2.45	−26.3	169
			middle	3.50	−23.2	149
			upper	5.78	−17.1	1308
16.0	11.7	1.5	lower	2.44	−28.1	171
			middle	3.50	−29.5	179
			upper	6.20	−21.7	1491

Table 2. Simulated gains of the first antenna with L1 = 16mm, L2 = 11.7mm, and S = 1mm at operating frequencies.

f (GHz)	$x-z$ plane gain (dBi)	$y-z$ plane gain (dBi)
2.45	1.79	1.97
3.50	0.64	2.08
5.80	1.57	2.35

Table 3. Measured gains of the first antenna with L1 = 16mm, L2 = 11.7mm, and S = 1mm at operating frequencies.

f (GHz)	$x-z$ plane gain (dBi)	$y-z$ plane gain (dBi)
2.45	2.46	2.80
3.50	1.02	3.50
5.80	5.20	6.45

The measured radiation patterns of the fabricated antenna are illustrated in Fig. 3(c) and 3(d) at 2.45 GHz, Fig. 4(c) and 4(d) at 3.5 GHz, and Fig. 5(c) and 5(d) at 5.8 GHz, respectively. The measured peak gains for testing frequencies at $x-z$ and $y-z$ planes of the fabricated antenna are listed in Table 3. There are discrepancies between the simulated and measured results which may occur because of the effect of the coaxial connector soldering process and fabrication tolerance.

2.3. **Experimental Results.** From the simulation results, we use the appropriate geometric parameters to fabricate the proposed antenna. To reach the operating frequencies

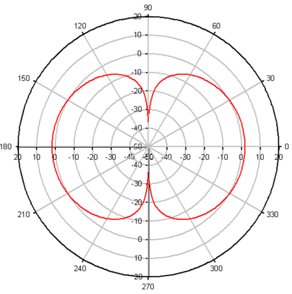

(a) $x - z$ plane, $f = 2.45$ GHz

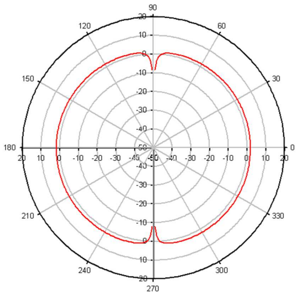

(b) $y - z$ plane, $f = 2.45$ GHz

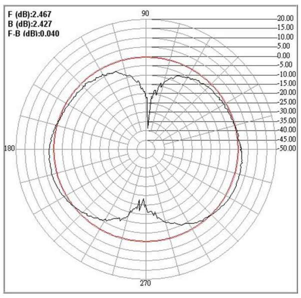

(c) $x - z$ plane, $f = 2.45$ GHz

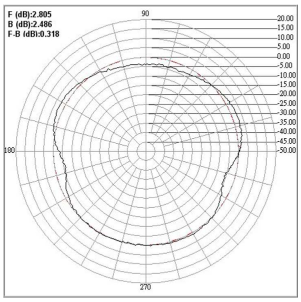

(d) $y - z$ plane, $f = 2.45$ GHz

FIGURE 3. Radiation patterns of the first antenna at 2.45 GHz. (a)(b): Simulation. (c)(d) Measurement.

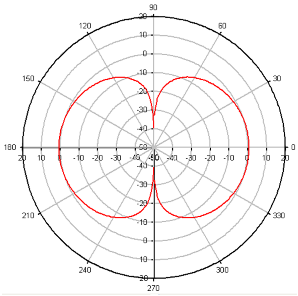

(a) $x - z$ plane, $f = 3.5$ GHz

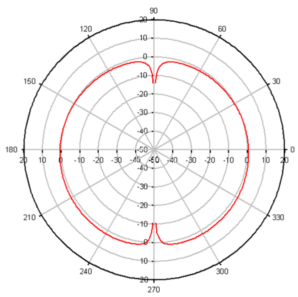

(b) $y - z$ plane, $f = 3.5$ GHz

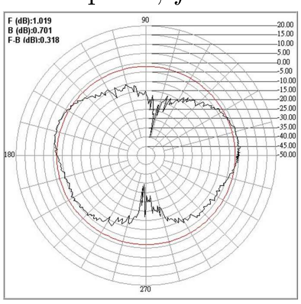

(c) $x - z$ plane, $f = 3.5$ GHz

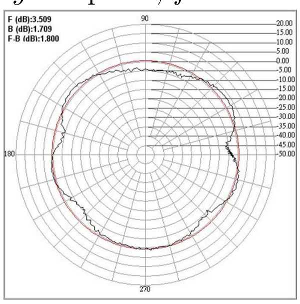

(d) $y - z$ plane, $f = 3.5$ GHz

FIGURE 4. Radiation patterns of the first antenna at 3.5 GHz. (a)(b): Simulation. (c)(d) Measurement.

covering 2.45/3.5/5.8 GHz, we choose L1 = 16mm, L2 = 11.7mm and S = 1mm to fabricate the desired antenna. The photography of fabricated antenna is demonstrated in Fig. 6. The curves of return loss against frequency of the simulated and fabricated antenna are illustrated in Fig. 7. Finally, the simulated and measured results are listed in

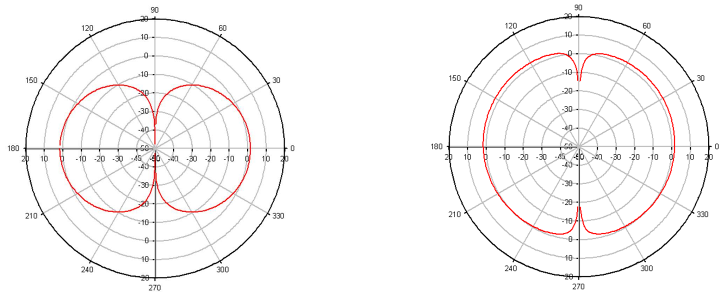

(a) $x - z$ plane, $f = 5.8$ GHz (b) $y - z$ plane, $f = 5.8$ GHz

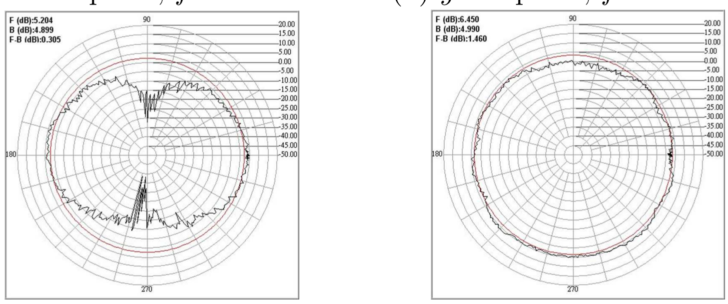

(c) $x - z$ plane, $f = 5.8$ GHz (d) $y - z$ plane, $f = 5.8$ GHz

FIGURE 5. Radiation patterns of the first antenna at 3.5 GHz. (a)(b): Simulation. (c)(d) Measurement.

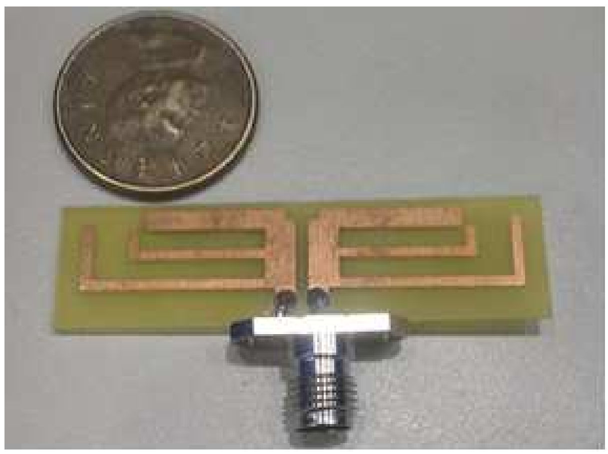

FIGURE 6. Photography of fabricated planar dipole antenna.

Table 4. From these data, we observe that the trend of simulated and measured operating frequency band and return loss are in good agreement. The measured impedance bandwidths of the fabricated antenna for return loss less than -10 dB at lower, middle and upper frequency band are 320 MHz, 230 MHz and 3160 MHz, respectively. The measured return loss and impedance bandwidth of the fabricated antenna represent the better performance than that in the simulation conditions.

From Figs. 3(d), 4(d) and 5(d), we can observe that the radiation patterns are almost omnidirectional in the $y - z$ plane. The omnidirectional antenna radiation pattern indicates that the fabricated antenna is good for mobile devices.

3. **The 0.9/1.8/2.45 GHz Antenna.**

Table 4. Simulated and measured results of the first antenna.

Condition	f_c (GHz)	RL (dB)	BW (MHz)
Simulation	2.45	−27.0	170
	3.50	−28.6	170
	6.00	−19.1	1435
Measurement	2.52	−27.3	320
	3.50	−26.0	230
	5.65	−31.6	3160

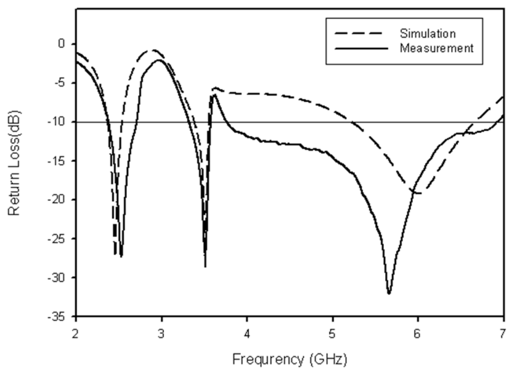

Figure 7. Simulated and measured return loss of the proposed antenna.

3.1. **Antenna Design.** The second antenna has a compact size of 43mm×20mm×1.6mm. Like the first antenna in Sec. 2, the planar dipole antenna structure is printed on a single metallic layer of FR4 dielectric substrate with the permittivity of 4.4 and thickness of 1.6mm. Configuration of the second antenna is depicted in Fig. 8. Three symmetric arms are etched on the metallic layer to create the operating frequency bands in Fig. 8. Points A and B are the feeding points of the planar dipole antenna. Similar to the counterparts of the first antenna, three parameters, including the lower arm length parameter L1, the middle arm length parameter L2, and the upper arm corner parameter S are adjusted to observe the variations with respect to the resonant frequency and impedance bandwidth.

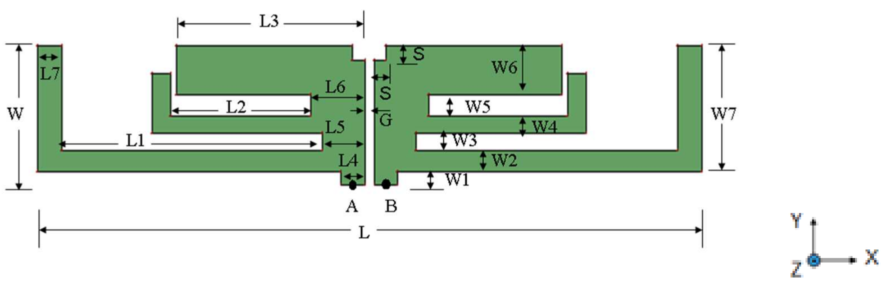

Figure 8. Configuration for the proposed TSAD antenna.

The dimension parameters of the proposed antenna shown in Fig. 8 are listed below.

- For the parameters in horizontal direction (x-direction): L3 = 31mm, L4 = 4mm, L5 = 7mm, L6 = 9mm, L7 = 4mm, and G = 0.5mm.
- For the parameters in vertical direction (y-direction): W = 20mm, W1 = 2mm, W2 = 3mm, W3 = 2.5mm, W4 = 2.5mm, W5 = 3mm, W6 = 7mm, and W7 = 18mm.

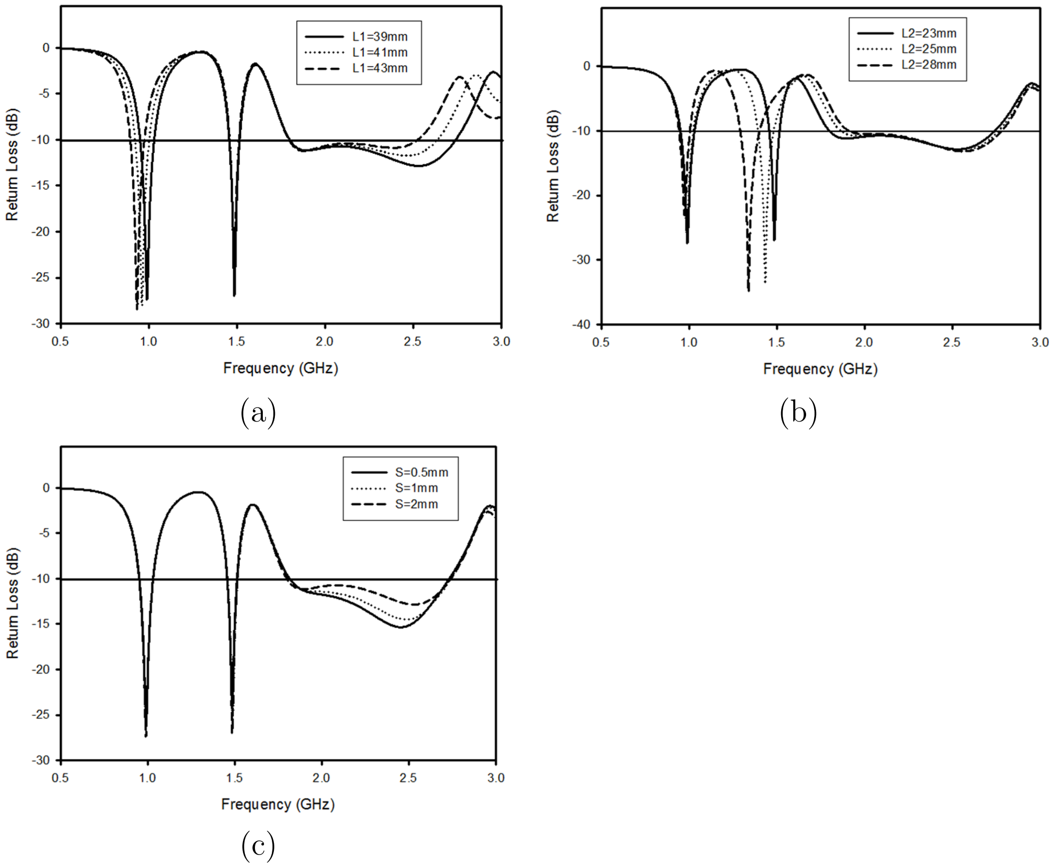

FIGURE 9. Simulated curves of return loss against frequency under different conditions. (a) By varying L1 with L2 = 23mm and S = 2mm. (b) By varying L2 with L1 = 39mm and S = 2mm. (c) By varying S with L1 = 39mm and L2 = 23mm.

In addition, the 50 ohm coaxial connector was adopted for testing.

3.2. **The Simulations.** We adopted various dimension parameters L1, L2 and S depicted in Fig. 8 of the TSAD antenna to observe the characteristic variations of these antennas. The numerical simulation and analysis for the TSAD antennas are performed using IE3D simulation software.

Simulation curves of return loss against frequency for varying the lower arm parameter L1 of the TSAD antenna with L2 = 23mm and S = 2mm are depicted in Fig. 9(a). Three obvious operating frequency bands are observed and the lower operating frequency gets slightly reduced with increasing the value of L1 in Fig. 9(a). Correspondingly, curves of return loss against frequency for varying the middle arm parameter L2 of the proposed antenna with L1 = 39mm and S = 2mm, and for varying the upper arm parameter S of the proposed antenna with L1 = 39mm and L2 = 23mm, are demonstrated in Fig. 9(b) and Fig. 9(c), respectively. In Fig. 9(b), like its counterparts in Fig. 9(a), with the increase of L2, the middle operating frequency gets reduced. In Fig. 9(c), there seems little influences to the operating frequencies with the increase of S. The lower, middle and upper operating frequency band simulated results are listed in Table 5. These simulated results include resonant frequency (f_c), return loss (RL), and impedance bandwidth (BW).

In order to design the second antenna operating at 0.9/1.8/2.45 GHz, we select the better size parameters L1 = 43mm, L2 = 23mm and S = 2mm to observe the radiation

Table 5. Simulated results for varying dimension parameters of the second antenna.

L1 (mm)	L2 (mm)	S (mm)	Frequency band	f_c (GHz)	RL (dB)	BW (MHz)
39.0	23.0	2.0	lower	0.99	−27.4	80
			middle	1.48	−26.8	58
			upper	2.53	−12.8	941
39.0	25.0	2.0	lower	0.98	−25.3	74
			middle	1.43	−33.4	90
			upper	2.59	−12.9	897
39.0	28.0	2.0	lower	0.97	−22.6	62
			middle	1.39	−34.5	110
			upper	2.59	−13.1	869
39.0	23.0	0.5	lower	0.99	−25.7	79
			middle	1.49	−23.9	55
			upper	2.44	−15.0	917
39.0	23.0	1.0	lower	0.99	−26.3	79
			middle	1.49	−25.0	58
			upper	2.51	−14.4	925
41.0	23.0	2.0	lower	0.96	−27.8	80
			middle	1.48	−26.3	55
			upper	2.53	−11.6	837
43.0	23.0	2.0	lower	0.93	−28.4	80
			middle	1.48	−25.9	53
			upper	2.44	−10.7	730

Table 6. Simulated gains of the second antenna with L1 = 43mm, L2 = 23mm, and S = 2mm at operating frequencies.

f (GHz)	$x-z$ plane gain (dBi)	$y-z$ plane gain (dBi)
0.90	1.93	1.94
1.80	1.51	2.12
2.45	1.98	2.66

Table 7. Measured gains of the second antenna with L1 = 43mm, L2 = 23mm, and S = 2mm at operating frequency.

f (GHz)	$x-z$ plane gain (dBi)	$y-z$ plane gain (dBi)
0.90	3.41	4.96
1.80	2.64	3.58
2.45	3.24	4.68

pattern of this TSAD antenna. The radiation patterns are computed using IE3D software for the proposed TSAD antenna. Figures 10(a) and 10(b) illustrate the simulated radiation patterns at 0.9 GHz. Figs. 11(a), 11(b) and Figs. 12(a), 12(b) present their counterparts at 1.8 GHz and 2.45 GHz, respectively.

The computed peak gains at the operating frequency obtained from the radiation patterns are arranged in Table 6. It can be observed that the radiation patterns are almost omnidirectional in the $y-z$ plane as depicted in Fig. 10(b), Fig. 11(b), and Fig. 12(b), respectively. From the simulation results, it is easy to find that the simulated return loss, impedance bandwidth and peak gain of the proposed TSAD antenna present the better performance, and it can be applicable at 0.9/1.8/2.45 GHz.

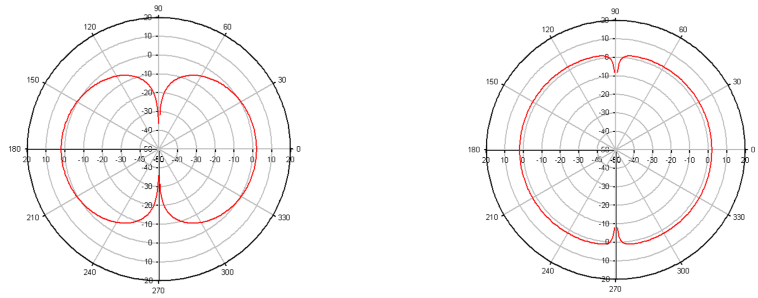

(a) $x - z$ plane, $f = 0.9$ GHz (b) $y - z$ plane, $f = 0.9$ GHz

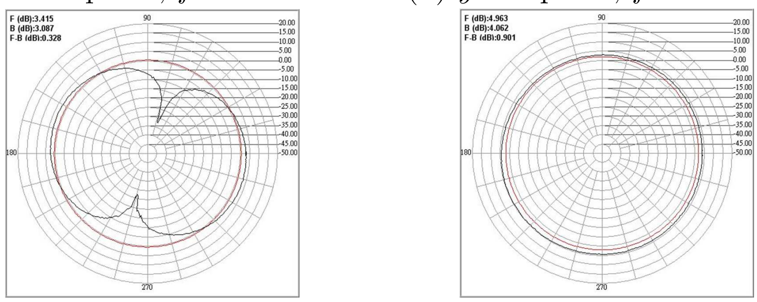

(c) $x - z$ plane, $f = 0.9$ GHz (d) $y - z$ plane, $f = 0.9$ GHz

FIGURE 10. Radiation patterns of the second antenna at 0.9 GHz. (a)(b): Simulation. (c)(d) Measurement.

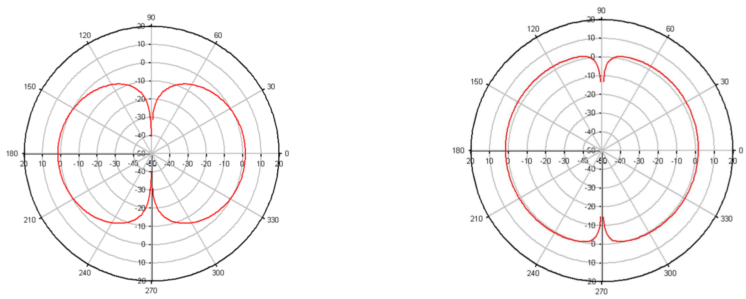

(a) $x - z$ plane, $f = 1.8$ GHz (b) $y - z$ plane, $f = 1.8$ GHz

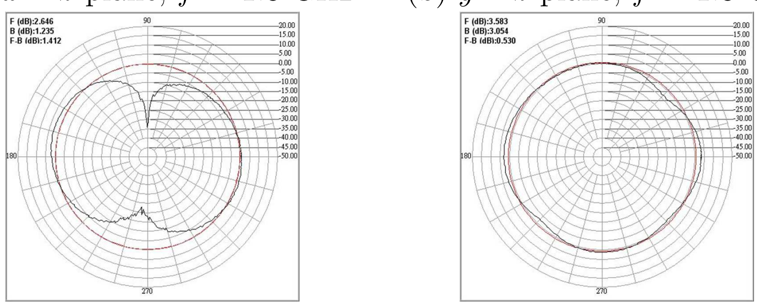

(c) $x - z$ plane, $f = 1.8$ GHz (d) $y - z$ plane, $f = 1.8$ GHz

FIGURE 11. Radiation patterns of the second antenna at 1.8 GHz. (a)(b): Simulation. (c)(d) Measurement.

Figures 10(c) and 10(d) depict the measured radiation patterns of the fabricated TSAD antenna with L1 = 43mm, L2 = 23mm, and S = 2mm at 0.9 GHz, Fig. 11(c) and 11(d) present their counterparts at 1.8 GHz, and Fig. 12(c) and 12(d) display their counterparts at 2.45 GHz, respectively. The measured peak gains for testing frequencies at $x - z$ and $y - z$ plane of the fabricated TSAD antenna are listed in Table 7.

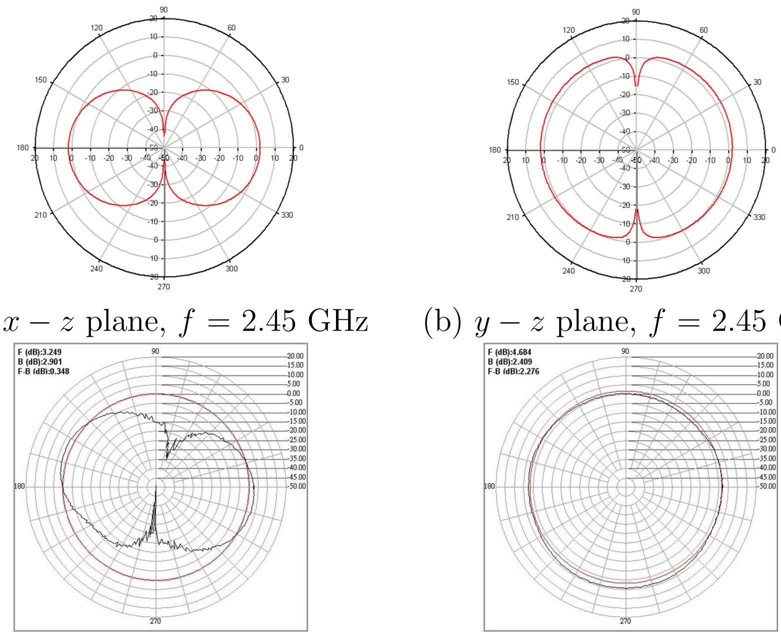

(a) $x - z$ plane, $f = 2.45$ GHz (b) $y - z$ plane, $f = 2.45$ GHz

(c) $x - z$ plane, $f = 2.45$ GHz (d) $y - z$ plane, $f = 2.45$ GHz

FIGURE 12. Radiation patterns of the second antenna at 2.45 GHz. (a)(b): Simulation. (c)(d) Measurement.

TABLE 8. Measured results of the second antenna at operating frequencies.

L1 (mm)	f_c (GHz)	RL (dB)	BW (MHz)
39.0	1.02	−27.8	106
	1.50	−28.0	80
	1.99	−16.3	931
41.0	0.96	−36.4	137
	1.50	−17.5	95
	2.38	−21.5	657
43.0	0.91	−29.5	122
	1.38	−23.8	69
	2.25	−17.6	799

3.3. **Experimental Results.** From the simulation results, we use the appropriate geometric parameters to fabricate the proposed TSAD antenna. To reach the operating frequencies covering 0.9/1.8/2.45 GHz, we choose L2 = 23mm and S = 2mm with varying L1 to fabricate the desired antennas. Figure 13 demonstrates the photography of the fabricated TSAD antennas. The curves of return loss against frequency of the fabricated antennas are illustrated in Fig. 14. The measured results are listed in Table 8. From these data, we observe that the measured operating frequency band and return loss have the same tendency as the simulated results. There are some discrepancies between the computed and measured results, and these may occur because of the effect of the coaxial connector soldering process and fabrication tolerance. The fabricated TSAD antenna with L1 = 43mm, L2 = 23mm and S = 2mm meets the requirement of the desired antenna that can be used at 0.9/1.8/2.45 GHz.

From Figs. 10(d), 11(d), and 12(d), we can observe that the radiation patterns are almost omnidirectional in the $y-z$ plane. The omnidirectional antenna radiation pattern indicates that the fabricated antenna is good for mobile devices. The measured peak gains

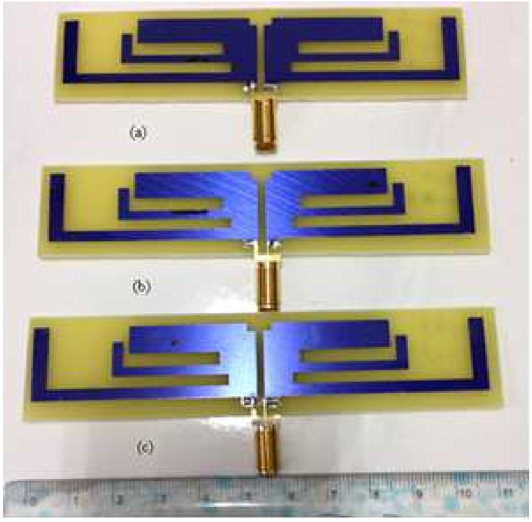

FIGURE 13. Photography of fabricated TSAD antennas. (a) L1 = 39mm. (b) L1 = 41mm. (c) L1 = 43mm.

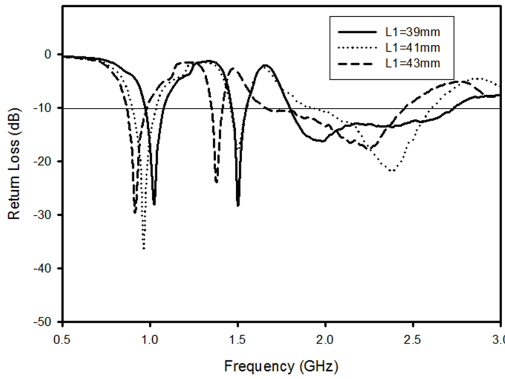

FIGURE 14. Measured curves of return loss against frequency for varying L1 of the fabricated TSAD antennas.

of the fabricated TSAD antenna at 0.9 GHz, 1.8 GHz and, 2.45 GHz are 4.96 dBi, 3.58 dBi, and 4.68 dBi, respectively. Therefore, the fabricated antenna can be used for GSM 0.9/1.8 GHz and RFID 0.9/2.45 GHz applications.

4. **Comparisons and Discussions.** With the similar design concepts, we present two antennas which can operate at triple-bands for different applications in wireless communications. Considering the maximal and minimal frequency bands, we take 5.8 GHz and 0.9 GHz as an instance. For 5.8 GHz, the half wavelength corresponds to 25.86 mm in the design of dipole antennas, and for 0.9 GHz, it corresponds to 166.67 mm. And this is the major reason for selecting L1, L2, and L3 in Fig. 1 and Fig. 8, respectively.

Here we also provide the current distribution patterns in Fig. 15 for the first antenna in Sec. 2, and in Fig. 16 for the second antenna in Sec. 3. We can observe that the patterns correspond with the desired frequency bands accordingly.

5. **Conclusions.** In this paper, we presented two fabricated triple-band planar dipole antennas for 2.45/3.5/5.8 GHz and 0.9/1.8/2.45 GHz applications. They exhibit simple structure and small in size. With the careful chosen of designed parameters of the

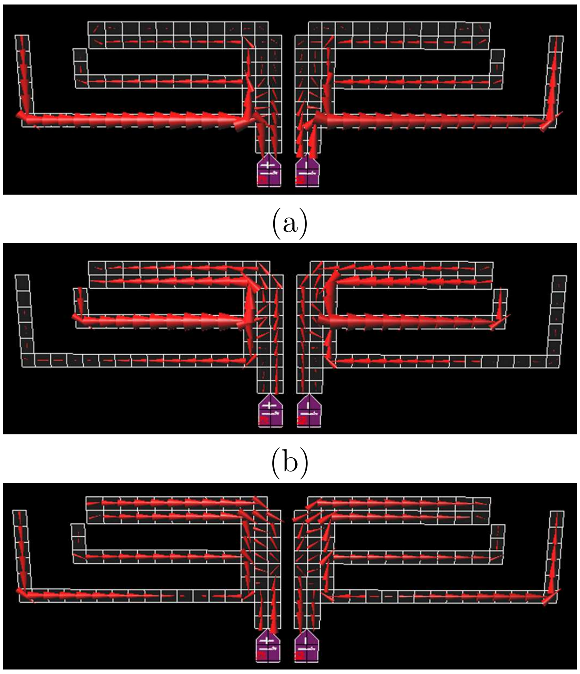

(a) (b) (c)

FIGURE 15. The current distribution patterns of the first antenna in Sec. 2. (a) At 2.45 GHz. (b) At 3.5 GHz. (c) At 5.8 GHz.

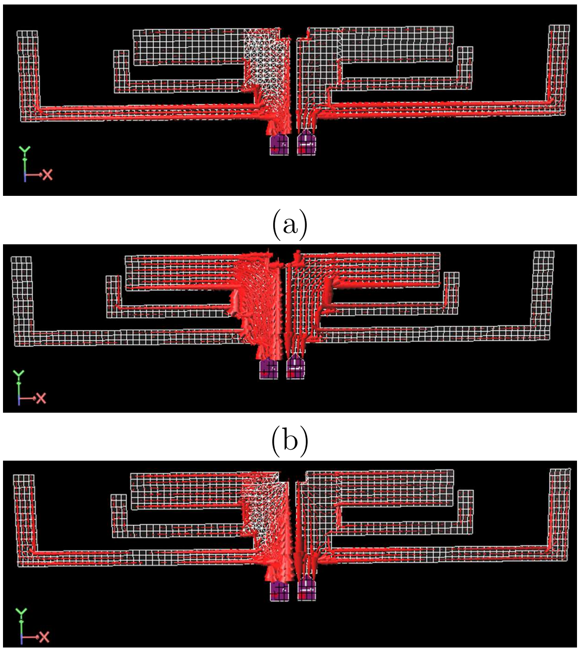

(a) (b) (c)

FIGURE 16. The current distribution patterns of the first antenna in Sec. 3. (a) At 0.9 GHz. (b) At 1.8 GHz. (c) At 2.45 GHz.

symmetric arm, operating frequencies would lie into the triple bands as designed. After the simulations with IE3D software, the two antennas are fabricated, and the measured results have high correlations with the simulated ones. Therefore, the performances of proposed antennas can be verified. Finally, the fabricated planar dipole antennas can be built as an on-board antenna, and this would reduce the manufacturing cost of a device.

Acknowledgment. The authors would like to thank Ministry of Science and Technology (Taiwan, R.O.C.) for supporting this paper under Grant No. MOST103-2221-E-390-018.

REFERENCES

[1] Y. Y. Lu, J. J. Jhu, and H.C. Huang, "Design of high gain planar dipole array antenna for WLAN application," *Int'l Conf. on Intell. Inform. Hiding and Multimedia Signal Proc.*, pp. 1–4, 2013.

[2] A. Khaleghi, "Dualband meander line antenna for wireless LAN communication," *IEEE Trans. Antennas and Propagation*, vol. 55, no. 3, pp. 1004–1009, Mar. 2007.

[3] C. M. Wu, C. N. Chiu, and C. K. Hsu, "A new nonuniform meandered and fork-type grounded antenna for triple-band WLAN applications," *IEEE Antennas and Wireless Propagation Letters*, vol. 5, no. 1, pp. 346–348, Dec. 2006.

[4] J. P. Zhang, Y. S. Xu, and W. D. Wang, "Ultra-wideband microstrip-fed planar elliptical dipole antenna," *Electronics Letters*, vol. 42, no. 3, pp. 144–145, Feb. 2006.

[5] Y. Y. Lu, S. C. Wei, and H. C. Huang, "Design of RFID antenna for 2.45GHz applications," *Int'l Conf. on Innovative Comp., Information and Control*, pp. 601–604, 2009.

[6] H. R. Lee and J. M. Woo, "Asymmetric planar dipole antenna on the surface of conducting plane for RFID tag," *Asia Pacific Microwave Conf.*, pp. 633–636, 2009.

[7] Y. Y. Lu, J. Y. Guo, and H. C. Huang, "Design of triple symmetric arms dipole antenna for 900/1800/2450MHz applications," *Int'l Conf. on Intell. Inform. Hiding and Multimedia Signal Proc.*, pp. 1–4, 2014.

[8] Y. C. Chen, P. T. Chiu, J. M. Tsai, and M. D. Chen, "A compact triple-band planar monopole antenna for WLAN and WiMAX applications," *Int'l Workshop on Antenna Technology*, pp. 311–314, 2013.

[9] W. S. Chen, *et al.*, "A small planar 4G antenna with a coupled-fed monopole and a directed-fed monopole for mobile handset application," *Asia Pacific Microwave Conf.*, pp. 334–336, 2012.

[10] Y. Y. Lu, J. Y. Guo, K. L. Chung, and H.C. Huang, "Design of triple-band planar dipole antenna," *Advances in Intelligent Systems and Computing*, vol. 297, pp. 465–473, 2014.

[11] Z. Srica, B. Ivsic, D. Bonefacic, "Dual-band microstrip antenna for GSM applications," *Proc. of ELMAR*, pp. 293–298, 2012.

[12] T. W. Chiou and K. L. Wong, "A compact dual-polarized aperture-coupled patch antenna for GSM 900/1800-MHz systems," *Asia Pacific Microwave Conf.*, pp. 95–98, 2005.

[13] S. Gupta, M. Ramesh, and A.T. Kalghatgi, "Design of optimized CPW fed monopole antenna for UWB applications," *Asia Pacific Microwave Conf.*, 2005.

[14] R. Chair, A. A. Kishk, and K. F. Lee, "Ultrawide-band coplanar waveguide-fed rectangular slot antenna," *IEEE Antennas and Wireless Propagation Letters*, vol. 3, no. 1, pp. 227–229, Dec. 2004.

[15] Y. Y. Lu, S. C. Wei, C. Y. Li, and H. C. Huang, "Design of 2.45GHz planar meander dipole antenna," *Int'l Conf. on Intell. Inform. Hiding and Multimedia Signal Proc.*, pp. 5–8, 2011.

[16] J. Grosinger, M. Fischer, "Evaluating on-body RFID systems at 900 MHz and 2.45GHz," *Int'l EURASIP Workshop on RFID Technology*, pp.52–58, 2012.

[17] P. Xu, Z. H. Yan, and C. Wang, "Multi-band modified fork-shaped monopole antenna with dual L-shaped parasitic plane," *Electronics Letters*, vol. 47, no. 6, pp. 364–365, Mar. 2011.

[18] W. Lin, Q. X. Chu, "A novel RFID tag antenna for matching complex impedances on 915 MHz and 2.45 GHz bands," *Asia Pacific Microwave Conf.*, pp. 2248–2251, 2010.

[19] Y. Y. Lu, C. Y. Li, and H. C. Huang, "Design of irregular width loop antenna for 2.45/5.2/5.8 GHz applications," *Int'l Conf. on Intell. Inform. Hiding and Multimedia Signal Proc.*, pp. 207–210, 2012.

[20] O. Ayop, M. K. A. Rahim, and T. Masri, "Planar dipole antenna with and without circular parasitic element," *Asia-Pacific Conf. on Applied Electromagnetics*, pp. 1–4, 2007.

[21] F. F. Dubrovka and D. O. Vasylenko, "A bell-shaped planar dipole antenna," *Int'l Conf. on Ultra-wideband and Ultrashort Impulse Signals*, pp. 82–84, 2006.